Remote Sensing of Environment 153 (2014) 40–49

Contents lists available at ScienceDirect

Remote Sensing of Environment

journal homepage: www.elsevier.com/locate/rse

Monitoring dry vegetation masses in semi-arid areas with MODIS SWIR bands

Damien Christophe Jacques [a,*], Laurent Kergoat [b], Pierre Hiernaux [b], Eric Mougin [b], Pierre Defourny [a]

[a] Earth and Life Institute, Université Catholique de Louvain, Belgium
[b] Geosciences Environnement Toulouse (GET, CNRS/UPS/IRD/CNES), Toulouse, France

ARTICLE INFO

Article history:
Received 14 March 2014
Received in revised form 26 July 2014
Accepted 28 July 2014
Available online xxxx

Keywords:
Dry vegetation
Mass
MODIS
Semi-arid areas
Sahel
Monitoring
Rangeland

ABSTRACT

Monitoring the mass of herbaceous vegetation during the dry season in semi-arid areas is important for a number of domains in ecology, agronomy, or economy and remote sensing offers relevant spatial coverage and frequency to that end. Existing remote sensing studies dedicated to dry herbaceous vegetation detection are mainly motivated by the assessment of soil tillage intensity and soil residue management, risk of soil erosion, and risk of wildfire linked to the mass of dead fuel. Few studies so far have dealt with monitoring of straw and litter degradation during the dry season over large areas while they are important fodder for livestock sustainability. MODIS band combinations (NBAR collection 5) were tested against a set of field measurements carried out over 20 rangeland sites from 2004 to 2011 in the Sahel. The best empirical linear models were obtained for indices using MODIS bands in the shortwave infrared domain (Band 6 centered at 1.6 μm, Band 7 centered at 2.1 μm), in particular with the Soil Tillage Index (STI). STI explained 66% of the variance of dry masses ($Mass = 3158(STI - 1.05)$, $r^2 = 0.66$, RMSE = 280 kg DM/ha, n = 232) for dry and intermediate season data. A regression is also proposed for year-round data ($Mass = 3371(STI - 1.06)$, $r^2 = 0.67$, RMSE = 352 kg DM/ha, n = 536). The strong inter-site and inter-annual variabilitieswere well captured and the decay rate was found consistent with grazing intensity and fire occurrence. The results imply that the STI can be applied to monitor the mass of dry tissues in the Sahel and potentially in many semi-arid areas.

© 2014 Elsevier Inc. All rights reserved.

1. Introduction

Semi-arid areas are characterized by a long dry season, during which annual plants die and perennial herbaceous plants often suffer drought by letting above-ground tissues dry while the below-ground parts survive. During the dry season, many physical and ecological processes, as well as some economical activities, interact with the amount and distribution of these above-ground dry tissues. Livestock sustainability for instance, depends on available fodder, which mostly consists of dry herbaceous plants. This resource varies throughout the year and from year to year. In the Sahel, for example, the extreme drought of 1984 resulted in very low plant production and extremely low dry-season fodder, which had severe impact on livestock survival and thus on pastoral population. In this context, assessing dry-season forage resources is a major concern and remote sensing offers relevant spatial coverage and frequency to that end. Frequent and accurate assessment of dry tissues is also very useful to studies of soil erosion, fire emissions biogeochemical cycles and surface energy budget (Barbosa, Stroppiana, Grégoire, & Cardoso Pereira, 1999; Samain et al., 2008; Shinoda, Gillies, Mikami, & Shao, 2011) in West Africa, but more generally in most arid and semi-arid areas worldwide (e.g. (Dregne, 2011)).

During the last decade, a number of remote sensing studies have addressed the detection of dry vegetation, pursuing different objectives: derivation of soil tillage intensity, soil conservation (Daughtry & Hunt, 2008; Daughtry, Hunt, Doraiswamy, & McMurtrey, 2005; Daughtry et al., 2006), evaluation of soil erosion risk and runoff (Arsenault & Bonn, 2005; Bannari, Chevrier, Staenz, & McNairn, 2007; Bergeron, 2000; Biard & Baret, 1997), evaluation of the risk of wildfire in relation to dead fuel proportion (Cao, Chen, Matsushita, & Imura, 2010; Elmore, Asner, & Hughes, 2005; Roberts et al., 2003) and improvement in land cover mapping (Guerschman et al., 2009; Peña-Barragán, Ngugi, Plant, & Six, 2011). The spectral signature of dry canopies and its application in the field has been extensively discussed by Nagler, Daughtry, & Goward(2000); Nagler, Inoue, Glenn, Russ, & Daughtry(2003) and Daughtry, Gallo, Goward, Prince, & Kustas(1992) among others. Few studies focused on dry season forage estimation, in terms of mass for instance (Ren & Zhou, 2012), and even fewer studies have tested monitoring methods efficient at large scale, since field or airborne spectroscopy or high resolution data from Landsat (Marsett et al., 2006; Serbin, Hunt, Daughtry, McCarty, & Doraiswamy, 2009; Zheng, Campbell, & de Beurs,

* Corresponding author.
E-mail address: damien.jacques@uclouvain.be (D.C. Jacques).

http://dx.doi.org/10.1016/j.rse.2014.07.027
0034-4257/© 2014 Elsevier Inc. All rights reserved.

2012) or Hyperion (Daughtry et al., 2006; Guerschman et al., 2009; Monty, Daughtry, & Crawford, 2008; Roberts et al., 2003) were used in most cases.

Different factors potentially impair the detection of dry vegetation masses.

1. The similarity between soil and dry vegetation spectral signatures (Gausman, Wiegand, Leamer, Rodriguez, & Noriega, 1975) as well as the diversity of the soil spectral signature, which depends on factors such as mineralogy, structure, texture, and moisture (Aase & Tanaka, 1991; Baret, Jacquemoud, & Hanocq, 1993; Serbin, Daughtry, Hunt, Brown, & McCarty, 2009).
2. The structure of the vegetation, depending on the species and on the canopy architecture (standing grasses or litter for instance) (Daughtry, Serbin, Reeves, Doraiswamy, & Hunt, 2010; Kokaly & Clark, 1999; Wanjura & Bilbro, 1986).
3. The biochemical composition and state (C/N ratio, water content, tissue aging, photosynthesis activity) (Daughtry & Hunt, 2008).
4. The impact of wild or controlled fires on spectral properties (Lewis et al., 2010).

Ideally, a dry-season forage index allowing the retrieval of the mass of plant tissues should cope with all these effects. Furthermore, it should be derived on a week-to-week basis to capture forage dynamics along the season.

The objective of the present study is to investigate the relationship that exists between several reflectances and indices and masses of standing straws and litter using MODIS data from TERRA and AQUA satellites. For that purpose, radiometric indices are evaluated, through empirical linear models, against a set of field measurements collected over 8 years for a network of sites in the Sahel. Furthermore, the sensitivity of mass retrieval to the structure of the vegetation (proportion of standing straws and litter), the season and thus the water content, the presence of photosynthetic vegetation, the soil background, and the burn scars are analyzed to determine the robustness of the method.

2. Background

2.1. Spectral characteristics of dry vegetation

The spectral regions mostly used to assess crop residue cover, litter or more generally dry or non-photosynthetic vegetation on the ground are the visible (VIS, 0.4–0.7 μm), near infrared (NIR, 0.7–1.2 Im) and shortwave infra-red (SWIR, 1.2–2.5 μm) domains. The use of the VIS–NIR domain is debated because of difficulties to distinguish dry vegetation from the underlying ground. Indeed, in this spectral region, soil and dry vegetation both display a wide range of spectral signatures, with soil reflectance being lower or higher than the dry vegetation is (Aase & Tanaka, 1991; Nagler et al., 2000; Nagler et al., 2003). The SWIR domain contains absorption features of dry vegetation at 1.7, 2.1 and 2.35 μm (Fig. 1). Elvidge(1990) has observed absorption features at 2.1 and 2.3 μm using Airborne Visible Infrared Imaging Spectrometer (AVIRIS) data over dry shrubs. Absorption in the SWIR has been associated with structural compounds as cellulose, hemicellulose and lignin since non-structural compounds as sugars and starches are already degraded by microorganisms in dry material (Elvidge, 1990; Roberts, Smith, & Adams, 1993; Roberts et al., 1990). As leaf water content increases, these absorption features are impacted by spectral properties of water (Kokaly, Asner, Ollinger, Martin, & Wessman, 2009; Kokaly & Clark, 1999; Serbin, Daughtry, Hunt, Brown, & McCarty, 2009).

2.2. Dry vegetation indices

The signature of dry matter compounds in the SWIR domain has fostered the emergence of various indices, most often for discriminating dry vegetation from green vegetation and soil background. Table 1 presents the formula of the indices described hereafter.

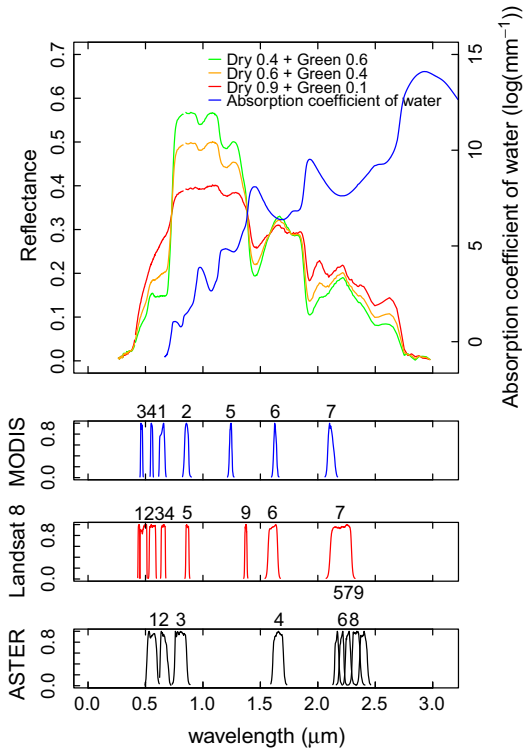

Fig. 1. Spectral signatures of areal mixtures of dry long grass collected early August and lawn grass picked on June, from the USGS digital spectral library (Clark et al., 2007) and the absorption coefficient of water (data from (Bertie & Lan, 1996)). Relative spectral responses of bands from MODIS, Landsat 8 and ASTER are also represented. Note that the MODIS band 7 (2.061–2.167 μm) falls into the absorption feature characteristic of dry vegetation at 2.1 μm. Other absorption features at 1.7 and 2.35 μm can be also observed on spectral signature of scene dominated by dry vegetation (red curve). (For interpretation of the references to color in this figure legend, the reader is referred to the web version of this article.)

Based on the spectral absorption feature at 2.1 μm, the Cellulose Absorption Index (CAI) was defined by Daughtry(2001). This index has been demonstrated many times to be suitable to detect dry vegetation

Table 1
Dry vegetation indices from literature. ρ_x is the reflectance of the wavelength in the band *x*. *TM*, *A*, *M* correspond to Landsat TM, ASTER, MODIS bands respectively. *a* and *b* are the slope and the intercept of the soil line in the corresponding spectral band domain. $L = 1 - 2a$. *NDSVI*. $(\rho_{TM5} - a\rho_{TM5})$. δ is the angle between the soil and the residue lines. ζ is the angle between the point to estimateand the soil line (see details in Biard & Baret (1997)).

Formula	References
Tested in the analysis	
$NDI5 = \frac{\rho_{TM4}-\rho_{TM5}}{\rho_{TM4}+\rho_{TM5}}$	McNairn and Protz (1993)
$NDI7 = \frac{\rho_{TM4}-\rho_{TM7}}{\rho_{TM4}+\rho_{TM7}}$	McNairn and Protz (1993)
$NDTI = \frac{\rho_{TM5}-\rho_{TM7}}{\rho_{TM5}+\rho_{TM7}}$	Van Deventer et al. (1997)
$NDSVI = \frac{\rho_{TM5}-\rho_{TM3}}{\rho_{TM5}+\rho_{TM3}}$	Marsett et al. (2006); Qi et al. (2002)
$Ratio = \frac{\rho_{M7}}{\rho_{M6}}$	Guerschman et al. (2009)
$STI = \frac{\rho_{M6}}{\rho_{M7}}$	Van Deventer et al. (1997)
Not tested in the analysis	
$SACRI = \frac{a(\rho_{TM4}-a\rho_{TM5}-b)}{(\rho_{TM5}+a\rho_{TM4}-ab)}$	Biard et al. (1995)
$MSACRI = C^{ste}\left[\frac{a(\rho_{ETM5}-a\rho_{ETM7}-b)}{(\rho_{ETM7}+a\rho_{ETM5}-ab)}\right]$	Bannari et al. (2000)
$SATVI = \frac{\rho_{TM5}-\rho_{TM3}}{(\rho_{TM5}+\rho_{TM3}+L)}(1+L)-\frac{\rho_{TM7}}{2}$	Marsett et al. (2006)
$DFI = 100\left(1-\frac{\rho_{M2}}{\rho_{M6}}\right)\frac{\rho_{M1}}{\rho_{M2}}$	Cao et al. (2010)
$CRIM = \frac{\tan(\delta)}{\tan(\zeta)} = \frac{\cos(\zeta)}{\cos(\delta)}\cdot\sqrt{\frac{1-\cos^2(\delta)}{1-\cos^2(\zeta)}}$	Biard and Baret (1997)
$CAI = 0.5(\rho_{2031}+\rho_{2211})-\rho_{2101}$	Daughtry (2001)
$LCA = 100[(\rho_{A6}-\rho_{A5})+(\rho_{A6}-\rho_{A8})]$	Daughtry et al. (2005)
$SINDRI = 100\left[\frac{\rho_{M6}-\rho_{M7}}{\rho_{M6}+\rho_{M7}}\right]$	Serbin, Hunt, Daughtry, McCarty, and Doraiswamy (2009)

(Daughtry et al., 2010; Nagler et al., 2003; Serbin, Daughtry, Hunt, Brown, & McCarty, 2009; Serbin, Hunt, Daughtry, McCarty, & Doraiswamy, 2009). Some studies have nuanced these results by showing that CAI was less accurate for crop residues cover less than 50% and for specific soil background (Bannari, Haboudane, & Bonn, 1999; Bannari et al., 2007; Chevrier, 2002). Nevertheless, CAI is a physical-based efficient index. Its major drawback is the need to obtain reflectance in very narrow bands in specific wavelengths. To date, only the EO-1 Hyperion sensor allows calculating CAI from space. Otherwise, airborne sensors as AVIRIS or field spectroradiometers have to be used, which are not suitable for large area monitoring.

In an attempt to use the spectral properties near the CAI signature, other indices, using the narrow SWIR bands from ASTER onboard TERRA (Fig. 1), have been designed: the Lignin Cellulose Absorption (LCA) (Daughtry et al., 2005) and the Shortwave Infrared Normalized Difference Residue Index (SINDRI) (Serbin, Hunt, Daughtry, McCarty, & Doraiswamy, 2009). ASTER however is not adapted for regional monitoring because of a low temporal frequency (16-day revisit) and a relatively small scene size. Furthermore it has to be tasked and the SWIR detector has been offline since April 2008 due to failure (JPL, 2012).

Guerschman et al.(2009) developed a linear unmixing approach for bare soil, photosynthetic and non-photosynthetic vegetation reflectance using the NDVI and the CAI, as proposed by Daughtry et al.(2005). They selected the MODIS bands the most closely related to CAI, using spectral libraries from field campaigns. The best result was shown to be the simple ratio between bands 7 (2.061–2.167 μm) and 6 (1.599–1.659 μm) in the SWIR domain. Other indices have been derived from MODIS data to detect dry tissues, most often relying on the SWIR bands. For instance, the Dead Fuel Index (DFI) developed by Cao et al.(2010) to discriminate dead fuel for fire prevention is in part built on the *B7/B6* ratio. The Normalized Difference Indices 5 and 7 (NDI5, NDI7, (McNairn & Protz, 1993)), Normalized Difference Tillage Index (NDTI, (Van Deventer, Ward, Gowda, & Lyon, 1997), (Zheng, Campbell, Serbin, & Daughtry, 2013), (Zheng et al., 2012)), Normalized Difference Senescent Vegetation Index (NDSVI, citeqi2002ranges, marsett2006remote), and Soil Tillage Index (STI, (Van Deventer et al., 1997)) are empirical indices built with different Landsat TM bands, adaptable to MODIS bands. Daughtry et al.(2010) have shown that most of these empirical indices are sensitive to the soil background. The soil line concept, a linear relationship between bare soil reflectance observed in two different wavebands (Baret et al., 1993), often used by 'green vegetation indices', has been also applied to 'dry vegetation indices' with the Soil Adjusted Crop Residue Index (SACRI) (Biard, Bannari, & Bonn, 1995), Modified Soil Adjusted Crop Residue Index (MSACRI, (Bannari, Haboudane, McNairn, & Bonn, 2000)) and Soil Adjusted Total Vegetation Index (SATVI, (Marsett et al., 2006)). Finally, Biard & Baret(1997) further developed the concept by initiating a residue line in the Crop Residue Index Multiband (CRIM). Since most of the MODIS based indices are relatively recent, and also because suitable ground data datasets are not easily gathered, the ability of these indices for large scale monitoring of dry season forage is not known. The sensitivity of the spectral signature in the SWIR domain to dry matter has been clearly demonstrated, the best results were obtained using space-borne hyperspectral (Hyperion) sensor or with ASTER that had specific bands in the SWIR, no longer functional. Finding a method suitable to sensors allowing high frequency observations (e.g. MODIS) is really of interest because they are those usually needed for monitoring over large areas.

3. Material and methods

3.1. Study site and field data

The network of sites extends from 14,5 N to 17,5 N and 2 W to 1 W in the Gourma region, which covers 90,000 km^2 south of the River Niger (Fig. 2). 22 permanent sites (Fig. 2) have been established to sample the diversity of precipitation regime, soil type, woody plant cover, and grazing pressure along a large latitude gradient (Hiernaux & Justice, 1986; Hiernaux et al., 2009; Mougin et al., 2009).

Dry season vegetation measurements were collected during an 8-year period (2004 to 2011), in addition to the measurements routinely collected in rainy season. Among these 22 sites, two sites with a tree cover exceeding 15% have been discarded (20, 21) as they are seasonally flooded forests (site numbers are from Hiernaux et al. (2009)). Four other sites are considered separately (8, 16, 22, 40) since they have a very shallow soil, being rocky outcrops or iron-pans with extremely low plant cover, which is itself largely dominated by trees and bushes. These sites are considered here to test the sensitivity of dry vegetation retrieval to the soil mineralogy. This leaves a fairly large dataset of 536 observations collected over 8 years and 16 different sites with sandy or loamy soil and a tree cover of less than 15%, spanning 2° of latitude.

Mass measurements (expressed in kilograms of dry matter per hectare) in the dry season follow the protocol used for green vegetation for the long term ecological survey (Hiernaux et al., 2009). Originally, these sites were selected to be homogeneous over 1 km^2. For each site, a 1 km line is sampled using a stratified random sampling. It combines 12 measurements of mass of straw and litter (dry weight) collected over 12×1 m^2. These samples represent three classes of vegetation density: 3 samples in the low and high class, 6 for the medium class. A sample in the bare soil class (mass $= 0$) is also added. The relative fractions of the four classes (high, medium, low and bare) are determined visually by careful inspection of every 1 m^2 segment along the 1 km line. The 1 km average mass is the sum of the class averaged masses weighted by the class relative fractions. This protocol has proven to be efficient for long-term monitoring of a large network of rangeland sites in the Sahel, for which inter-site variability and inter-annual variability can be very large (Dardel et al., 2014a,b; Hiernaux, 1996). The relative contribution of standing straw and litter to the total mass has been estimated visually.

Pastoral Sahel is dominated by annual grasses and dicotyledons. In the Gourma area, the dry season usually starts around the September 15 and ceases near June 15 (Frappart et al., 2009), with significant inter-annual variability in rain distribution within the wet season. This period has been separated in two parts for analysis purpose: the intermediate period, between the September 15 and the October 15 (referred to as intermediate season in figures), during which the vegetation can be found dry as well as green depending on rainfall and floristic composition, and the rest of the dry season between the October 15 and the June 15 (referred to as dry season in figures). The period from June 15 to September 15 is referred asthe wet season.

3.2. Remote-sensing data

The MODerate resolution Imaging Spectroradiometer (MODIS) onboard TERRA and AQUA satellites has a large spatial coverage, a high frequency of revisit time and data free access making it suitable for an application to the Sahelian context. The MODIS Nadir BRDF-adjusted reflectance (NBAR) product (MCD43A4, collection 5) provides every 8 days a normalized reflectance corrected for bidirectional and atmospheric effects, based on reflectance data collected over a 16-day period (Schaaf et al., 2002). The spatial resolution is 500 m. For each 1 km field site, the pixel which is the closest to the site center is extracted (http://daac.ornl.gov/cgi-bin/MODIS/GLBVIZ_1_Glb/modis_subset_order_global_col5.pl). NBAR data are interpolated through time to match the exact day of the field measurement.

3.3. Data analysis

Several indices have been tested, specifically NDI5, NDI7, NDTI, STI, and NDSVI, using equivalent MODIS bands. Indices using the soil line concept (SACRI, MSACRI, SATVI, CRIM) are not considered because the aim of the study is to find a method as simple as possible and applicable easily to large area. Using soil line requires a specific calculation for each

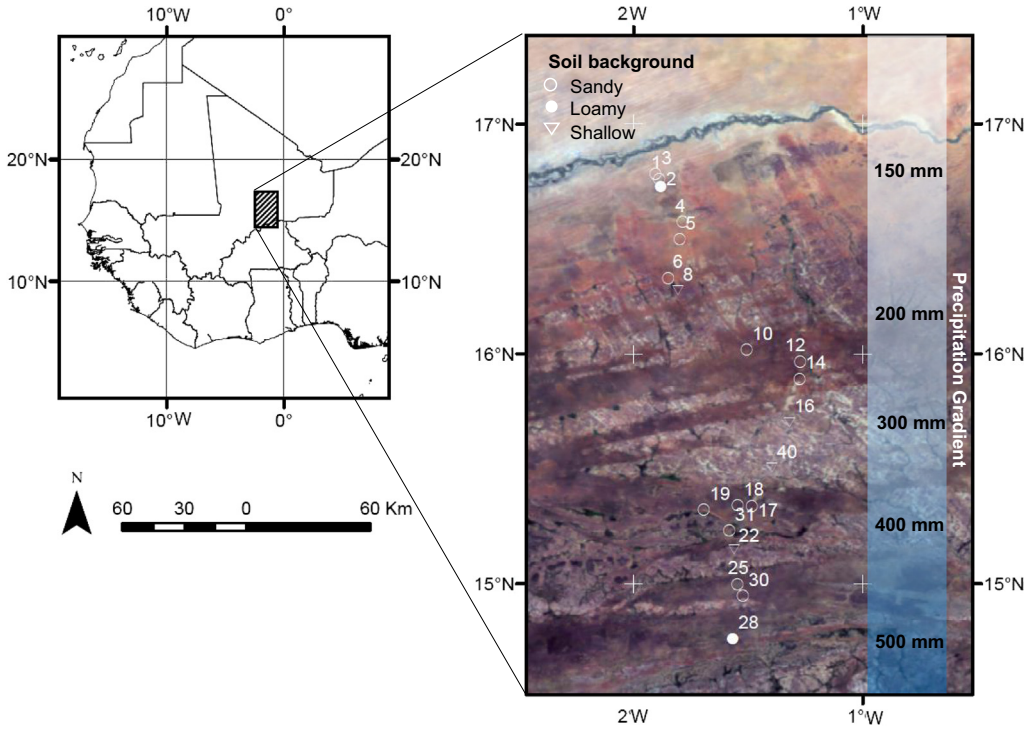

Fig. 2. The 22 field measurement sites in the Gourma region (Mali) displayed over a MODIS composite. Site numbers are from (Hiernaux et al., 2009).

site; therefore the method has been discarded. Moreover, due to the necessity of having narrow bands in specific wavelengths, indices using ASTER data (LCA, SINDRI) could not be computed with MODIS bands (Fig. 1). On the other hand, individual spectral bands (1–7) have been tested for the purpose of isolating any potential spectral region more sensitive to dry vegetation than others. Finally, the different combinations of simple difference, simple ratio and normalized difference between two of the first seven MODIS bands have been also tested in order to highlight a possible index that has not yet been identified in the literature.

Empirical relationships compute by linear regressions with herbaceous dry mass measured in the field as the dependent variable are applied to all indices. The performance of the models is compared using the coefficient of determination (r^2) and the root mean square error (RMSE).

Sensitivity of the selected index to the proportion of standing straws and litter, the season and thus the water content and the presence of photosynthetic vegetation (wet, intermediate or dry periods), the soil background (sandy, loamy or rocky) and the burn scars are systematically analyzed. Although it was not the primary objective of this study, the selected method has also been applied on data for the entire year and compared with the NDVI under the same conditions.

4. Results

4.1. Selection of the best combination of bands

The performance of the 10 best combinations of bands is presented in Table 2 for the two periods concerned by dry vegetation, namely the intermediate period (September 15 to October 15) and the dry season (October 15 to June 15) pooled together. All regressions have very high significant p-values ($p < 0.0001$), coefficient of determination (r^2) ranging from 0.67 to 0.62 and RMSE from 277 to 297 kg of DM/ha. Four of five indices found in the literature are present in these 10 best combinations (STI, NDI7, NDTI, and B7/B6 simple ratio). Note that we used the same index names when changing Landsat TM/ETM + bands 1, 2, 3, 4, 5, and 7 to respectively MODIS bands 3, 4, 1, 2, 6 and 7 in computing indices keeping in mind that bandwidth is slightly different. All the retained combinations use band 7 (2.061–2.167 μm), which is located in the spectral region of the ligno-cellulose absorption feature (Fig. 1). Considering the minor difference of r^2 and RMSE between band 7 (ranked as 11th, 0.61, 301 kg of DM/ha) and the best index (0.67, 277 kg of DM/ha), it seems that band 7 alone largely contributes to the relationship with the dry herbaceous mass for this time period. However, as it will be demonstrated below, using band 7 alone as a proxy of mass does not capture the fire effect on dry mass in a completely satisfying manner.

When the dry season is considered separately, thus excluding data from September 15 to October 15, the combinations of B7 and B6 result in the best models of dry herbaceous mass (Table 3). The RMSE is slightly smaller and the coefficient of determination is slightly lower than when the dry and intermediate seasons are combined.

The relationship for wet season data provides larger RMSE and slightly higher r^2. The bands B1, B3, B4 or B5 are preferred than B6 in some of the best combinations (Table 4). This is in line with the expected signature of green plant tissues over bright soils. Despite a well established sensitivity to green leaf area, the NDVI does not appear in the 10 best combinations for mass retrieval (25th, $r^2 = 0.54$ and RMSE = 459).

Table 2
Parameters of linear regressions between indices and mass data (RMSE expressed in kg of DM/ha) combining dry season and intermediate period measurements (September 15 to June 15, n = 232).

Literature	Index	r^2	RMSE
–	B5/B7	0.67	277
STI	B6/B7	0.66	280
–	(B5 − B7)/(B5 + B7)	0.66	280
NDTI	(B6 − B7)/(B6 + B7)	0.65	283
–	B7/B5	0.65	284
ratio	B7/B6	0.64	287
–	B2/B7	0.64	287
NDI7	(B2 − B7)/(B2 + B7)	0.64	290
–	B2 − B7	0.63	291
–	B7/B2	0.62	297

Table 3
Parameters of linear regressions between indices and mass data (RMSE expressed in kg of DM/ha) for dry season measurements only (October 15 to June 15, n = 193).

Literature	Index	r^2	RMSE
STI	B6/B7	0.59	238
NDTI	(B6 − B7)/(B6 + B7)	0.59	239
ratio	B7/B6	0.59	240
–	B5/B7	0.58	244
–	(B5 − B7)/(B5 + B7)	0.57	244
–	B7/B5	0.57	245
–	B6 − B7	0.55	250
–	B5 − B7	0.54	255
–	B2 − B7	0.52	259
–	B4 − B7	0.52	259

Table 5
Parameters of linear regressions between indices and mass data (RMSE expressed in kg of DM/ha) throughout the year measurements (n = 536).

Literature	Index	r^2	RMSE
STI	B6/B7	0.67	352
NDTI	(B6 − B7)/(B6 + B7)	0.66	356
–	B7	0.66	357
–	(B5 − B7)/(B5 + B7)	0.66	359
ratio	B7/B6	0.65	361
–	B7/B5	0.65	363
–	B4 − B7	0.65	363
–	B3 − B7	0.63	365
–	B5/B7	0.63	371
–	B1 − B7	0.63	371

When all mass data are pooled together, the B6 and B7 combinations stand out as the best predictors of vegetation mass (Table 5), and B7 is included in all the ten best combinations.

The ratio between band 6 and 7, referred to as STI, is retained for the rest of the analysis. The equivalent Landsat-based STI has proven successful for crop residue discrimination (Van Deventer et al., 1997) and its reciprocal, as it has been discussed above, has been used to estimate fractional non-photosynthetic vegetation (Guerschman et al., 2009). Using a band ratio eliminates some disturbances in the signal, and it can be applied to daily MODIS reflectance (rather than an 8-day composite) in case high temporal resolution is needed. According toTables 2 to 5, we acknowledge that several ratio combinations, based on bands 6 and 7, could have been selected, like *B7/B6* or *(B6 − B7)/(B6 + B7)*, because they share relatively similar performances.

4.2. Effect of vegetation status and soil background

The linear regression of STI against herbaceous mass for the dry and intermediate seasons is represented in Fig. 3a. The mass values range between 0 and 2396 kg DM/ha. There is no strong evidence of saturation in the *(STI,mass)* relationship over this range. The regression relies on the following equation:

$$Mass = 3158 \times STI - 3316 \quad (1)$$

which can be written as

$$Mass = 3158 \times (STI - 1.05) \quad (2)$$

where *Mass* is the herbaceous mass (kg DM/ha) and *STI* is the Soil Tillage Index.

The ratio between standing straw and litter is a potential source of variation of the *(STI,mass)* relationship, because of differences in canopy geometry and spectral properties of tissue. Fig. 3c shows the value of this ratio for each observation. The ratio of standing straw versus total mass appears to be at best a secondary effect. When the percentage of standing straw is high, the linear model may tend to slightly underestimate the mass and when the litter is dominant, the opposite occurs. In most cases however, the proportion of standing vegetation and litter was assessed visually at each sampling plot, a method that may lead to substantial measurement error. Some caution is thus required.

Data from the sandy soil sites and loamy soil sites (Fig. 3a) do not form distinct clusters. The soil effect has been further tested by including some barren soils in the analysis (Fig. 3b). Among them, rocky outcrops, mostly dark sandstone, schists and iron pans, clump close to the x-axis, meaning that STI can be higher for a very low herbaceous mass. Some shallow soil sites are covered by scattered sand or loam bars allowing some plants to grow. These sites tend to fit the (*STI*, *mass*) regression of Fig. 3b, whereas really bare rocky soils do not. Such rocky soils could be filtered out thanks to their flat seasonal dynamic and low values of NDVI or STI.

The primary objective of this study is the retrieval of dry season vegetation mass. It turns out that the STI is also well correlated when data dominated by green tissues are included (Table 5).

$$Mass = 3371 \times STI - 3574 \quad (3)$$

which can be written as

$$Mass = 3371 \times (STI - 1.06) \quad (4)$$

The slope of Eq. 4 is slightly larger than for Eq. 2, which is partly caused by a subset wet season data showing low mass (less than 400 kg DM/ha) and STI ranging from 1.1 to 1.3. That is consistent with the idea that the correlation of STI to mass may involve a correlation to the plant area index. In the early growing season, the ratio of canopy mass to canopy surface is increasing, since plants progressively build stems. There is a possibility that STI increases faster than mass does, at the beginning of the wet season. Indeed, STI and NDVI are linearly related during the wet season (Fig. 4) and it is known that NDVI increases much faster than mass in pastoral Sahel in the early growing season (Mbow, Fensholt, Rasmussen, & Diop, 2013). In addition the effect of water absorption is strong in the SWIR range and is more important for the band 7 (2200 m^{-1}) than for band 6 (498 m^{-1}), which could potentially affect the STI. During approximatively the ten days that follow germination, the water content of the vegetation is high (close to 80%) and then decreases toward 40% at peak biomass. Caution has to be used in the early growing season.

4.3. Time series and maps

Fig. 5 represents time series of the STI, scaled with Eq. 3 (all seasons data), and in situ mass for four contrasted sites. Site 17 (Fig. 5a) is a typical sandy soil site. The herbaceous layer at growing season peak is more or less continuous, whereas woody vegetation is scattered, with a total tree and bush cover reaching 3%. The site is located in the proximity of permanent water bodies and it is therefore grazed year-round, which

Table 4
Parameters of linear regressions between indices and mass data (RMSE expressed in kg of DM/ha) for wet season measurements only (June 15 to September 15, n = 324).

Literature	Index	r^2	RMSE
–	B1 − B7	0.68	382
–	B7	0.67	390
–	B4 − B7	0.66	395
STI	B6/B7	0.66	398
–	(B5 − B7)/(B5 + B7)	0.66	398
–	B3 − B7	0.65	396
NDTI	(B6 − B7)/(B6 + B7)	0.65	399
–	B7/B5	0.65	402
ratio	B7/B6	0.65	404
–	B6	0.65	404

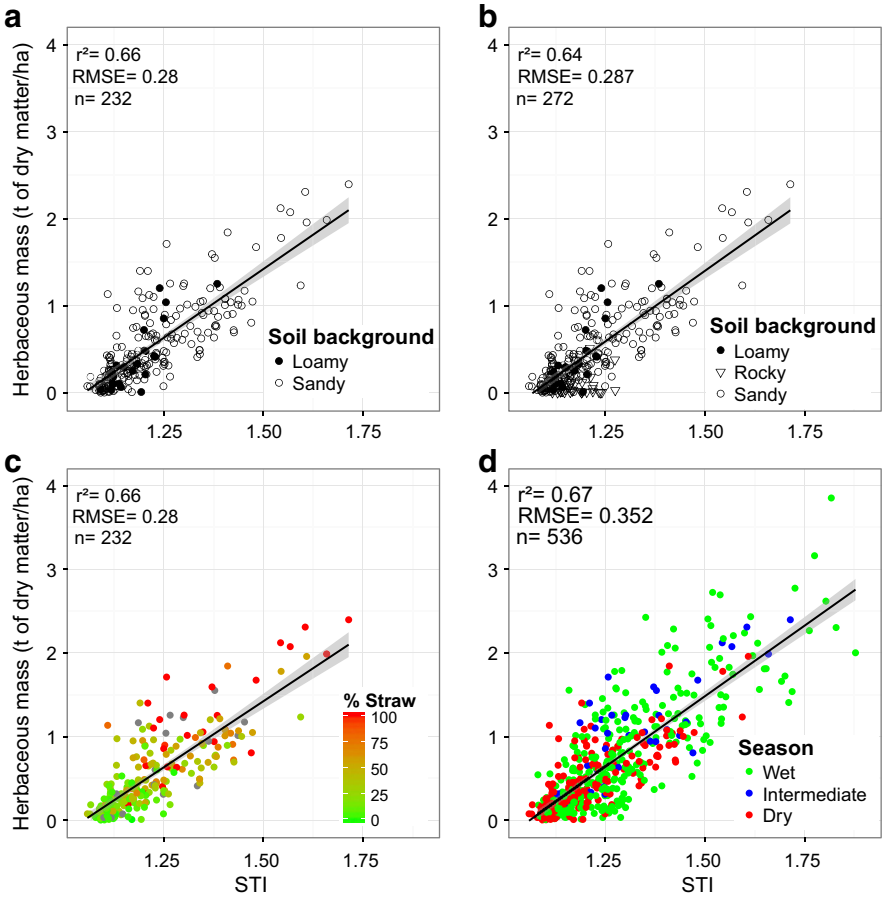

Fig. 3. Linear regression of STI against dry herbaceous mass (kg of dry matter/ha) for (a) dry and intermediate seasons (September 15 to June 15), (b) dry and intermediate seasons including rocky sites, (c) dry and intermediate seasons (September 15 to June 15) with color points (from green to red) indicating the % of standing vegetation (% Straw), gray points correspond to missing data, (d) sites with loamy and sandy soils, for the whole year. The gray area surrounding the regressionlines shows the 95% confidence interval. (For interpretation of the references to color in this figure legend, the reader is referred to the web version of this article.)

is not the case for sites 5 and 30. The decrease of the vegetation mass at the beginning of the dry season is more rapid for relatively intensively grazed sites (like 17), which is well reflected by STI dynamics. For instance, on the time series of site 5 (Fig. 5b), where dry season grazing is less intense due to the lack of water nearby, neither STI nor mass data shows a rapid decay. The average STI and total plant production are lower than for site 17 during these years. A relatively slow decrease

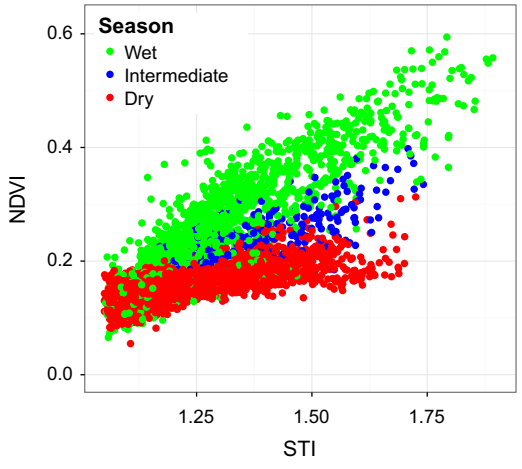

Fig. 4. Compared values of STI and NDVI during the 2000–2011 over 16 sites with loamy and sandy soil (n = 8958).

in the early dry season is more apparent, for at least 2004, 2007 and 2011 on site 30. Site 8 (Fig. 5d) is an illustration of a rocky outcrop where almost nothing grows. The expected signal is a straight line with only minor deviations, and this is what it is observed on the time series. STI has a rather constant value, higher than the lowest values for sites 17 and 5 at the end of the dry season. Another important observation on site 17 is the fire scar effect during the 2005 dry season, identified by a rapid decrease of STI, followed by a plateau lasting until the growth of the vegetation in the next rainy season. This phenomenon is illustrated also on the time series of site 30 (Fig. 5c) which is prone to fire, and not to grazing. The resulting time-series of mass data and STI both display 'square' irregular forms, because the herbaceous mass stays high during the dry season, since grazing pressure is very low, except when a fire occurs, which brings dry tissue mass to zero and STI to bare soil value. The site was partially burned in 2008–2009 and 2009–2010 which lead to intermediate STI values.

When bands 6 and 7 are scrutinized separately, the post fire periods result in a slow increase at both wavelengths (Fig. 6). This is not in line with the dynamics of dry tissues observed in situ after a fire. Since band 6 and band 7 increase in a similar way, the STI rapidly falls to a bare soil value and keep constant afterwards. This is consistent with the fact that the post-fire reflectances are mixtures of bare ground and black char reflectance (Lewis et al., 2010) with diminishing fraction of black char. Both bare ground and black char show a flat spectral signature in B6 and B7, which explains why STI correctly predicts no-mass values. STI has an advantage over band 7 alone in fire prone areas.

In order to characterize the spatial consistency of the index, a series of maps is represented on Fig. 7. They picture the region around the

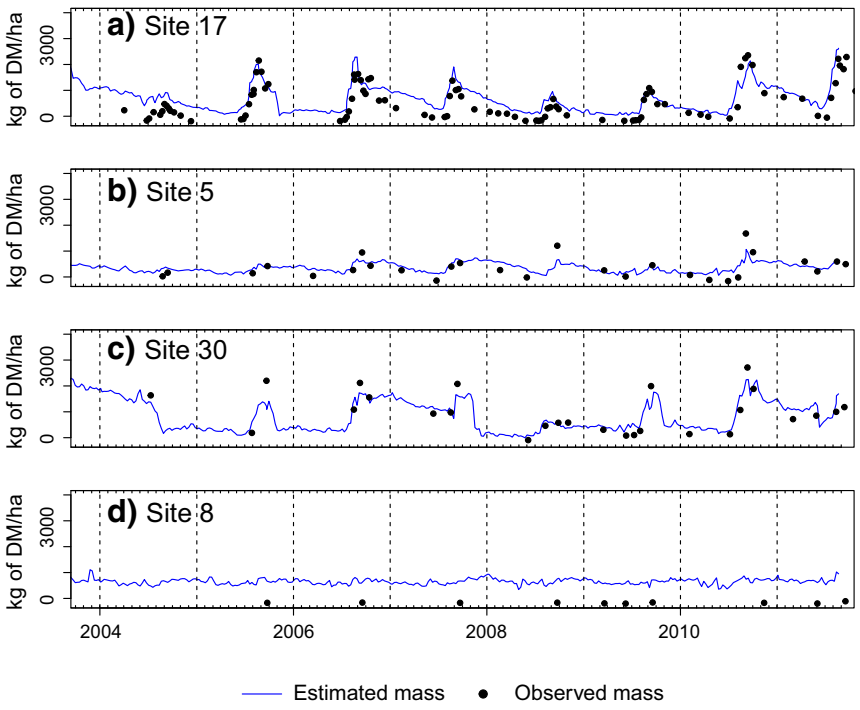

Fig. 5. Time series of estimated mass with Eq. 4, and in situ mass measurements of 4 contrasted sites. Site 17 (a) is intensively grazed, Site 5 (b) is little grazed, Site 30 (c) is prone to fire and Site 8 (d) is a rocky outcrop.

Agoufou permanent pond, starting before the 2006 rainy season. The north of the area is partially occupied by shallow soils, where almost no herbaceous vegetation grows, as it can be seen both in rainy season NDVI and on the land cover classification. For this land surface type, STI values stay low and roughly constant throughout the whole year. In the southern area, STI values decrease throughout the dry season, after the rapid burst corresponding to the growth of annual grasses and forbs during the rainy period. The decrease of the dry season STI is not spatially homogeneous. It is consistent with the spatial distribution of grazing pressure, since, for instance, large patches of dry vegetation persist far from the ponds. Fire scars (contoured in red in the last panel of Fig. 7) are also easily identifiable as instantaneous areas of low STI values, which stay low after the fire until the next rainy season. Note that the influence of water is also well marked by high STI values on areas cover by water.

5. Discussion

The STI provides a good retrieval of the herbaceous dry mass during the dry season, over a significant range of values (0–2500 kg DM/ha). These data span the typical range of pastoral rangeland dry season mass in the Sahel and more largely of many semi-arid rangelands. Within this range, no saturation of STI at high mass values was detected, implying that a linear relation can be used, which is of interest. STI fulfills most conditions to enable dry season monitoring of herbaceous mass that were listed in the introduction. In particular, a unique regression can be used in the presence of some green vegetation, during the transition season when green and dry tissues coexist. Therefore, an assessment of the 'start of dry season' value can be obtained, together with a dry season evolution, which is important for monitoring and managing purposes. The evaluation of the (*STI*,*mass*) regression over a large set of data indicates that 66% of the variance of dry season mass is explained with MODIS SWIR data. Such a result is in fact close to what is obtained for the widely-used methods retrieving vegetation production with integrated NDVI, when several years and sites are considered (see for instance (Dardel, Kergoat, Hiernaux, Mougin, et al., 2014b) and references therein for pastoral Sahel). Some of the scatter is caused by random errors in the 1 km field estimations. Indeed, mass varies in space within a 1 km site, and this variability is not completely captured by the sampling protocol. This could leave room for reducing scattering in (*STI*, *mass*) relationship with even more intensive field measurements. However, the real strength of the equations that we propose here comes

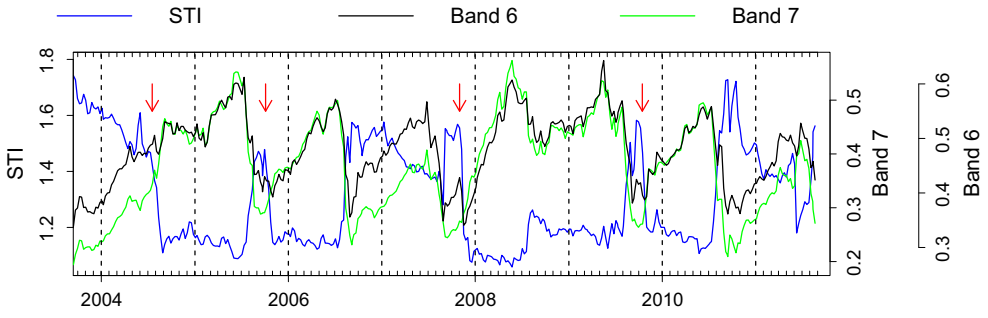

Fig. 6. Time series of STI and its component (reflectance in B6 and B7) for the site 30, prone to fire. Red arrows indicate the approximate date of fire. (For interpretation of the references to color in this figure legend, the reader is referred to the web version of this article.)

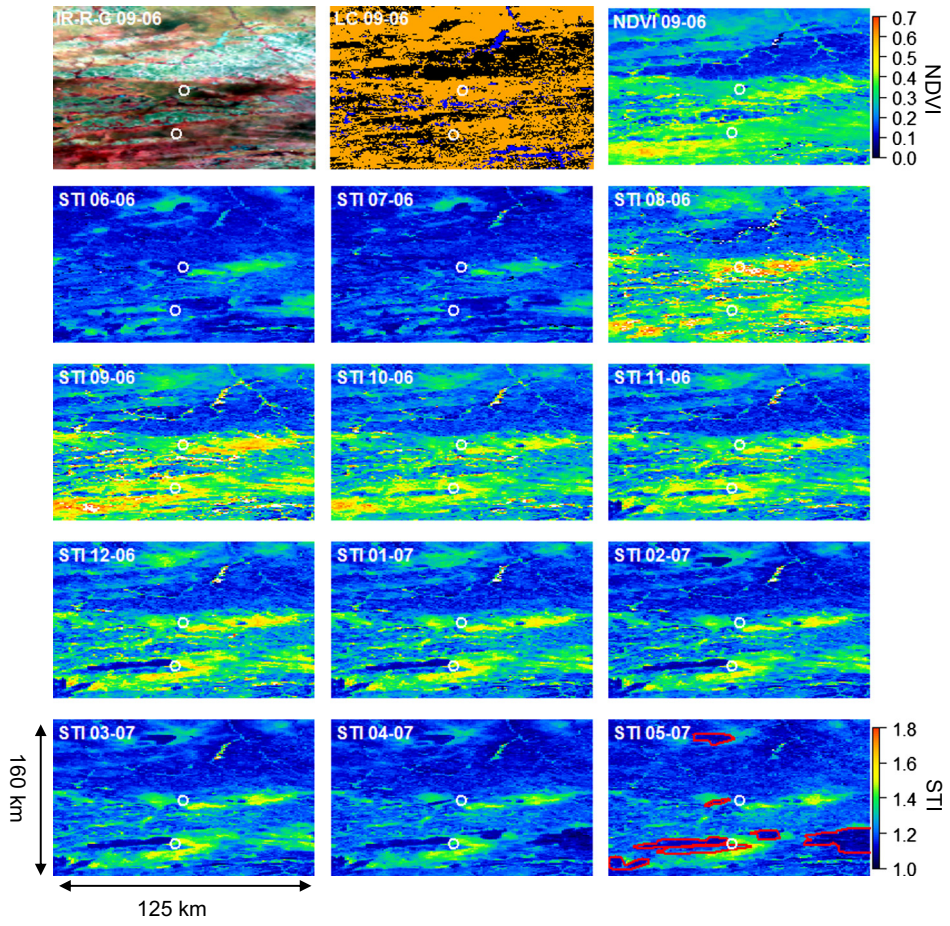

Fig. 7. Series of maps of STI around Site 17 and Site 30 (north and south white symbols, respectively) based on MODIS images over the 2006–2007 period. The upper row figures R-G-B and NIR-R-G color composites. LC is for Land Cover. It is a maximum likelihood classification, with black showing rocky outcrops and other shallow soils, blue corresponding to open water and flooded areas and orange corresponding to sandy and loamy deep soils. The next four rows show how STI varies in space and time. Burnt areas have been highlighted in red in the 05–07 map. The dates are expressed as mm-yy. (For interpretation of the references to color in this figure legend, the reader is referred to the web version of this article.)

from the wide ranges of sites, of dates and the long period of time that the field data provide. The variance explained is also comparable to the results of Ren & Zhou(2012), who estimated senesced biomass of desert steppe in Inner Mongolia using field spectrometric data. The best results with the CAI reaching a coefficient of determination of 0.67 from 155 in-situ observations.

Although it is not the primary focus of our study, the year-round equation predicting mass with STI would benefit from further investigation of the relationship with the specific leaf weight (leaf dry weight per unit area). The mass to surface ratio changes much less at the end of the growing season, during the intermediate and dry season (unpublished data), than during the early growing season. This probably contributes to the stability of the (*STI*,*mass*) relation through time, with an exception during the early growing season during which the water content has also been taken into account. In addition to the retrieval of herbaceous mass, we can expect a good retrieval of dry vegetation fraction cover also. This would be in line with the results of Guerschman et al.(2009), who demonstrated that the ratio *B7*/*B6* (reciprocal of STI) was the best combination to emulate the CAI and to predict dry vegetation cover fraction in an Australian grassland. The *B7*/*B6* ratio was selected because multiple linear regression $B7/B6 = x + y.\,NDVI + z.\,CAI$, gave a z/y very close to 1, implying thereby that the sensitivity of *B7*/*B6* is almost identical to NDVI and CAI. Under the hypothesis that CAI and NDVI are respectively perfect indices for dry and green vegetation cover, these results suggest that the ratio *B7*/*B6* (and its inverse, the STI) performs equally well during the intermediate period. The effect of soil moisture, which is expected to increase STI, has not been detected in our dataset. Surface soil moisture decreases very rapidly over Sahelians sandy soils, especially under clear-sky conditions thanks to rapid drainage and rapid drying of the top soil, often in a few hours (e.g. (Samain et al., 2008)). As a result, there are few occurrences of MODIS clear sky images over wet soil in the region, if any. Soil moisture effect is furthermore attenuated by the NBAR time-averaging. However, STI time profile might need to be filtered when using the whole-year (*STI*,*mass*) relationship, especially in more rainy areas.

The proposed index is suited to herbaceous-dominated landscapes. The sensitivity of STI to tree leaves mass or crop mass was not tested. From literature and first analysis of spectral signatures, there are reasons to expect significant relationships of STI with these variables, in terms of non-photosynthetic cover fraction. The slope and intercept of the relation of STI to mass, however, may well be different.

One caveat has to be kept in mind: some dark rocks and open water bodies have to be filtered out for large scale herbaceous mass estimates, which is relatively easy based on seasonal course of reflectances and absolute values over these targets. Overall, the soils in our study area are relatively bright (Samain et al., 2008). The (*STI*,*mass*) regression potentially applies to grass dominated ecosystems over bright soil, which includes pastoral Sahel but also many semi-arid areas worldwide.

6. Conclusion

It has been demonstrated that the ratio of MODIS bands 6 and 7, the Soil Tillage Index, can be used to assess herbaceous mass during the dry season with a good accuracy and robustness in the Sahel. A linear

regression was successfully applied during the dry season, including a transition period when dry and green plants coexist (66% of dry mass variance explained). Although it was not the primary objective of this study, it turns out that the STI is also well correlated when data dominated bygreen tissues are considered (67% of dry mass variance explained), although with some caveats especially in the early growing season and in case of wet soils. Seasonal and inter-annual variabilities of dry season plant mass have been monitored with the STI. The influence of dry-season grazing on dry mass decay, the influence of climate variability on plant production, as well as the abrupt changes caused by fire were well identified. The retrieval of dry season herbaceous mass has many applications, starting with forage monitoring, but also fire emissions estimates and monitoring of plant protection against wind erosion. Our results imply that STI can be applied to monitor the mass of dry vegetation tissues in many semi-arid areas.

Acknowledgment

We would like to thank all the reviewers for their relevant comments and suggestions that helped in improving the overall quality of the paper. Support from PNTS (PAILLASAT project, grantPNTS-2012-04), Système d'Observation AMMA-CATCH and ANRCAVIARS through grant ANR-12-SENV-0007 are acknowledged. This research was also partly funded by the Belgian National Fund for Scientific Research through a FRIA grant. We thank Mamadou Diawara (GET/Ecology lab from Bamako University) and Nogmana Soumaguel (IRD Bamako) for field measurements and Jose Gomez-Dans (UCL) for his interesting comments on the impact of leaf and soil water content. We also thank Françoise Guichard, who pointed the strong effect of litter on field measurement of broad-band albedo, which triggered this study.

References

Aase, J., & Tanaka, D. (1991). Reflectances from four wheat residue cover densities as influenced by three soil backgrounds. *Agronomy Journal*, *83*(4), 753–757.

Arsenault, E., & Bonn, F. (2005). Evaluation of soil erosion protective cover by crop residues using vegetation indices and spectral mixture analysis of multispectral and hyperspectral data. *Catena*, *62*(2–3), 157–172.

Bannari, A., Chevrier, M., Staenz, K., & McNairn, H. (2007). Potential of hyperspectral indices for estimating crop residue cover. *Revue Télédétection*, *7*, 447–463.

Bannari, A., Haboudane, D., & Bonn, F. (1999). Potentiel des mesures multispectrales pour la distinction entre les résidus de cultures et les sols nus sous-jacents. *Fourth International Airborne Remote Sensing Conference and Exhibition. Vol. 21.* (pp. 6–24). Ottawa, Ontarion, Canada: ERIM International.

Bannari, K., Haboudane, D., McNairn, H., & Bonn, F. (2000). Modified soil adjusted crop residue index (MSACRI): A new index for mapping crop residue. *Geoscience and Remote Sensing Symposium, 2000. Proceedings. IGARSS 2000. IEEE 2000 International*, *Vol. 7*. (pp. 2936–2938). IEEE.

Barbosa, P.M., Stroppiana, D., Grégoire, J. -M., & Cardoso Pereira, J. M. (1999). An assessment of vegetation fire in Africa (1981–1991): Burned areas, burned biomass, and atmospheric emissions. *Global Biogeochemical Cycles*, *13*(4), 933–950.

Baret, F., Jacquemoud, S., & Hanocq, J. (1993). The soil line concept in remote sensing. *Remote Sensing Reviews*, *7*(1), 65–82.

Bergeron, M. (2000). *Caractérisation du recouvrement végétal et des pratiques agricoles à l'aide d'une image TM de Landsat au nord du Viêt Nam.* (Master's thesis). Département de géographie et télédétection, Faculté des lettres et sciences humaines, Université de Sherbrooke.

Bertie, J. E., & Lan, Z. (1996). Infrared intensities of liquids XX: The intensity of the OH stretching band of liquid water revisited, and the best current values of the optical constants of H2O (l) at 25C between 15,000 and 1 cm^{-1}. *Applied Spectroscopy*, *50*(8), 1047–1057.

Biard, F., Bannari, A., & Bonn, F. (1995). SACRI (Soil Adjusted Crop Residue Index): An indice utilisant le proche et le moyen infrarouge pour la détection des residues de cultures de mais. *Proc. 17th Canadian symp. On remote sensing* (pp. 417–423). Ottawa: Canadian Remote Sensing Soc.

Biard, F., & Baret, F. (1997). Crop residue estimation using multiband reflectance. *Remote Sensing of Environment*, *59*(3), 530–536.

Cao, X., Chen, J., Matsushita, B., & Imura, H. (2010). Developing a MODIS-based index to discriminate dead fuel from photosynthetic vegetation and soil background in the Asian steppe area. *International Journal of Remote Sensing*, *31*(6), 1589–1604.

Chevrier, M. (2002). *Potentiel de la télédétection hyperspectrale pour la cartographie des résidus de cultures.* (Master's thesis). Ottawa (Ontario): Department of Geography, University of Ottawa.

Clark, R. N., Swayze, G. A., Wise, R., Livo, K. E., Hoefen, T. M., Kokaly, R. F., & Sutley, S. J. (2007). *USGS digital spectral library splib06a.* VA: US Geological Survey Reston.

Dardel, C., Kergoat, L., Hiernaux, P., Grippa, M., Mougin, E., Ciais, P., & C-C, N. (2014a). *Rain-use-efficiency: What it tells about the conflicting Sahel greening and Sahelian paradox, Remote Sensing 6, 3446–3474.*

Dardel, C., Kergoat, L., Hiernaux, P., Mougin, E., Grippa, M., & Tucker, C. (2014b). Re-greening Sahel: 30 years of remote sensing data and field observations (Mali, Niger). *Remote Sensing of Environment*, *140*, 350–364.

Daughtry, C. (2001). Discriminating crop residues from soil by shortwave infrared reflectance. *Agronomy Journal*, *93*, 125–131.

Daughtry, C., Doraiswamy, P., Hunt, E., Stern, A., McMurtrey, J., III, Prueger, J., et al. (2006). Remote sensing of crop residue cover and soil tillage intensity. *Soil and Tillage Research*, *91*(1–2), 101–108.

Daughtry, C., Gallo, K., Goward, S., Prince, S., & Kustas, W. (1992). Spectral estimates of absorbed radiation and phytomass production in corn and soybean canopies. *Remote Sensing of Environment*, *39*(2), 141–152.

Daughtry, C., & Hunt, E., Jr. (2008). Mitigating the effects of soil and residue water contents on remotely sensed estimates of crop residue cover. *Remote Sensing of Environment*, *112*(4), 1647–1657.

Daughtry, C., Hunt, E., Jr., Doraiswamy, P., & McMurtrey, J., III (2005). Remote sensing the spatial distribution of crop residues. *Agronomy Journal*, *97*, 864–871.

Daughtry, C., Serbin, G., Reeves, J., Doraiswamy, P., & Hunt, E. (2010). Spectral reflectance of wheat residue during decomposition and remotely sensed estimates of residue cover. *Remote Sensing*, *2*(2), 416–431.

Dregne, H. E. (2011). Soils of arid regions. *Vol. 6*, Elsevier.

Elmore, A., Asner, G., & Hughes, R. (2005). Satellite monitoring of vegetation phenology and fire fuel conditions in Hawaiian drylands. *Earth Interactions*, *9*(21), 1–21.

Elvidge, C. (1990). Visible and near infrared reflectance characteristics of dry plant materials. *International Journal of Remote Sensing*, *11*(10), 1775–1795.

Frappart, F., Hiernaux, P., Guichard, F., Mougin, E., Kergoat, L., Arjounin, M., Lavenu, F., Koité, M., Paturel, J. -E., & Lebel, T. (2009). Rainfall regime across the Sahel band in the Gourma region, Mali. *Journal of Hydrology*, *375*(1), 128–142.

Gausman, H., Wiegand, A., Leamer, C., Rodriguez, R. R., & Noriega, J. R. (1975). Reflectance differences between crop residues and bare soils. *Soil Science Society of America Journal*, *39*(4), 752.

Guerschman, J., Hill, M., Renzullo, L., Barrett, D., Marks, A., & Botha, E. (2009). Estimating fractional cover of photosynthetic vegetation, non-photosynthetic vegetation and bare soil in the Australian tropical savanna region upscaling the EO-1 Hyperion and MODIS sensors. *Remote Sensing of Environment*, *113*(5), 928–945.

Hiernaux, P. (1996). *The crisis of Sahelian pastoralism: Ecological or economic? Vol. 39*, ILRI (aka ILCA and ILRAD).

Hiernaux, P., & Justice, C. (1986). Suivi du développement végétal au cours de l'été 1984 dans le Sahel Malien. *International Journal of Remote Sensing*, *7*(11), 1515–1531.

Hiernaux, P., Mougin, E., Diarra, L., Soumaguel, N., Lavenu, F., Tracol, Y., & Diawara, M. (2009). Sahelian rangeland response to changes in rainfall over two decades in the Gourma region, Mali. *Journal of Hydrology*, *375*(1), 114–127.

JPL, N. (2012). HyspIRI Mission Study. http://hyspiri.jpl.nasa.gov/

Kokaly, R., Asner, G., Ollinger, S., Martin, M., & Wessman, C. (2009). Characterizing canopy biochemistry from imaging spectroscopy and its application to ecosystem studies. *Remote Sensing of Environment*, *113*, S78–S91.

Kokaly, R. F., & Clark, R. (1999). Spectroscopic determination of leaf biochemistry using band-depth analysis of absorption features and stepwise multiple linear regression. *Remote Sensing of Environment*, *67*(3), 267–287.

Lewis, P., Quaife, T., Disney, M., Gomez-Dans, J., Wooster, M., Pinty, B., & Roy, D. (2010). *Radiative transfer modelling for the characterisation of natural burnt surfaces.* Tech. rep.: University College London.

Marsett, R., Qi, J., Heilman, P., Biedenbender, S., Watson, M., Amer, S., Weltz, M., Goodrich, D., & Marsett, R. (2006). Remote sensing for grassland management in the arid southwest. *Rangeland Ecology & Management*, *59*(5), 530–540.

Mbow, C., Fensholt, R., Rasmussen, K., & Diop, D. (2013). Can vegetation productivity be derived from greenness in a semi-arid environment? Evidence from ground-based measurements. *Journal of Arid Environments*, *97*, 56–65.

McNairn, H., & Protz, R. (1993). Mapping corn residue cover on agricultural fields in Oxford County, Ontario, using Thematic Mapper. *Canadian Journal of Remote Sensing*, *19*(2), 152–159.

Monty, J., Daughtry, C., & Crawford, M. (2008). Assessing crop residue cover using hyperion data. *Geoscience and remote sensing symposium, 2008. IGARSS 2008. IEEE International*, *Vol. 2*. (pp. II-303). IEEE.

Mougin, E., Hiernaux, P., Kergoat, L., Grippa, M., De Rosnay, P., Timouk, F., Le Dantec, V., Demarez, V., Lavenu, F., Arjounin, M., et al. (2009). The AMMA-CATCH Gourma observatory site in Mali: Relating climatic variations to changes in vegetation, surface hydrology, fluxes and natural resources. *Journal of Hydrology*, *375*(1), 14–33.

Nagler, P., Daughtry, C., & Goward, S. (2000). Plant litter and soil reflectance. *Remote Sensing of Environment*, *71*(2), 207–215.

Nagler, P., Inoue, Y., Glenn, E., Russ, A., & Daughtry, C. (2003). Cellulose absorption index (CAI) to quantify mixed soil-plant litter scenes. *Remote Sensing of Environment*, *87*(2–3), 310–325.

Peña-Barragán, J. M., Ngugi, M. K., Plant, R. E., & Six, J. (2011). Object-based crop identification using multiple vegetation indices, textural features and crop phenology. *Remote Sensing of Environment*, *115*(6), 1301–1316.

Qi, J., Marsett, R., Heilman, P., Bieden-bender, S., Moran, S., Goodrich, D., & Weltz, M. (2002). RANGES improves satellite-based information and land cover assessments in southwest United States. *Eos, Transactions American Geophysical Union*, *83*(51), 601–606.

Ren, H., & Zhou, G. (2012). Estimating senesced biomass of desert steppe in Inner Mongolia using field spectrometric data. *Agricultural and Forest Meteorology*, *161*, 66–71.

Roberts, D., Dennison, P., Gardner, M., Hetzel, Y., Ustin, S., & Lee, C. (2003). Evaluation of the potential of Hyperion for fire danger assessment by comparison to the airborne visible/infrared imaging spectrometer. *IEEE Transactions on Geoscience and Remote Sensing*, *41*(6), 1297–1310.

Roberts, D., Smith, M., & Adams, J. (1993). Green vegetation, nonphotosynthetic vegetation, and soils in AVIRIS data. *Remote Sensing of Environment*, *44*(2–3), 255–269.

Roberts, D., Smith, M., Adams, J., Sabol, D., Gillespie, A., & Willis, S. (1990). Isolating woody plant material and senescent vegetation from green vegetation in AVIRIS data. *2nd Airborne Visible/Infrared Imaging Spectrometer (AVIRIS) Workshop* (pp. 42–57). Pasadena, CA: JPL.

Samain, O., Kergoat, L., Hiernaux, P., Guichard, F., Mougin, E., Timouk, F., Lavenu, F., et al. (2008). Analysis of the in situ and MODIS albedo variability at multiple timescales in the Sahel. *Journal of Geophysical Research*, *113*, D14119.

Schaaf, C., Gao, F., Strahler, A., Lucht, W., Li, X., Tsang, T., et al. (2002). First operational BRDF, albedo nadir reflectance products from MODIS. *Remote Sensing of Environment, Elsevier*(83), 135–148.

Serbin, G., Daughtry, C. S., Hunt, E. R., Brown, D. J., & McCarty, G. W. (2009). Effect of soil spectral properties on remote sensing of crop residue cover. *Soil Science Society of America Journal*, *73*(5), 1545–1558.

Serbin, G., Hunt, E., Daughtry, C., McCarty, G., & Doraiswamy, P. (2009). An improved ASTER index for remote sensing of crop residue. *Remote Sensing*, *1*(4), 971–991.

Shinoda, M., Gillies, J., Mikami, M., & Shao, Y. (2011). Temperate grasslands as a dust source: Knowledge, uncertainties, and challenges. *Aeolian Research*, *3*(3), 271–293.

Van Deventer, A., Ward, A., Gowda, P., & Lyon, J. (1997). Using thematic mapper data to identify contrasting soil plains and tillage practices. *Photogrammetric Engineering & Remote Sensing*, *63*(1), 87–93.

Wanjura, D. F., & Bilbro, J., Jr. (1986). Ground cover and weathering effects on reflectance of three crop residues. *Agronomy Journal*, *78*(4), 694–698.

Zheng, B., Campbell, J. B., & de Beurs, K. M. (2012). Remote sensing of crop residue cover using multi-temporal Landsat imagery. *Remote Sensing of Environment*, *117*, 177–183.

Zheng, B., Campbell, J., Serbin, G., & Daughtry, C. (2013). Multitemporal remote sensing of crop residue cover and tillage practices: A validation of the minNDTI strategy in the United States. *Journal of Soil and Water Conservation*, *68*(2), 120–131.